On the multistream approach of relativistic Weibel instability. II. Bernstein-Greene-Kruskal-type waves in magnetic trapping

Alain Ghizzo

On the multistream approach of relativistic Weibel instability. II. Bernstein-Greene-Kruskal-type waves in magnetic trapping

A. Ghizzo

Citation: Physics of Plasmas **20**, 082110 (2013); doi: 10.1063/1.4817751
View online: https://doi.org/10.1063/1.4817751
View Table of Contents: http://aip.scitation.org/toc/php/20/8
Published by the American Institute of Physics

On the multistream approach of relativistic Weibel instability. II. Bernstein-Greene-Kruskal-type waves in magnetic trapping

A. Ghizzo
Institut Jean Lamour UMR 7163, Université de Lorraine, BP 239 F-54506 Vandoeuvre les Nancy, France

(Received 16 May 2013; accepted 15 July 2013; published online 9 August 2013)

The stationary state with magnetically trapped particles is investigated at the saturation of the relativistic Weibel instability, within the "multiring" model in a Hamiltonian framework. The multistream model and its multiring extension have been developed in Paper I, under the assumption that the generalized canonical momentum is conserved in the perpendicular direction. One dimensional relativistic Bernstein-Greene-Kruskal waves with deeply trapped particles are addressed using similar mathematical formalism developed by Lontano *et al.* [Phys. Plasmas **9**, 2562 (2002); Phys. Plasmas **10**, 639 (2003)] using several streams and in the presence of both electrostatic and magnetic trapping mechanisms. © *2013 AIP Publishing LLC*.
[http://dx.doi.org/10.1063/1.4817751]

I. INTRODUCTION

Nearly 50 years ago, Bernstein, Greene, and Kruskal in Ref. 1 discovered a class of nonlinear equilibria (BGK waves) in collisionless plasmas. Owing the existence of particle trapping process in the wave's potential, BGK modes require a kinetic Vlasov-Poisson description. In these studies, plasma is able to support stationary large amplitude spatially periodic structures exhibiting "holes" in phase space. Such BKG waves can be excited experimentally today.[2] The formation of the holes in the phase space density corresponds to the presence of a small population of trapped particles but which plays here the fundamental role in the stopping of the Landau damping. Such an equilibrium is described by a distribution function depending only on the energy of particles. In numerical Vlasov-Poisson experiments presented in Ref. 3, such BGK waves have been found to be unstable, although they first appear at the initial stage of a two-stream homogeneous plasma. But in all cases, the interaction of vortices brings a coalescence until only one vortex subsists. In fact, the stabilization is here related to the finite size of the system, since a system exhibiting only one BGK structure is indeed marginally stable. Another point observed in Vlasov simulations (see Ref. 4) is the possibility to obtain holes having frequency well below the plasma frequency ω_p due to the tendency of holes to merge. In particular, the coalescence of two electron holes leads to a wave vector divided by a typical value close to two (due to pair-wise vortex merging) and thus the frequency of the driven mode kv_k is not quite divided by two but jumps from a value of $\omega \geq \omega_p$ (given by the standard Bohm-Gross dispersion relation) to a value found well below ω_p. Such an aspect of the instability shows the major role played by kinetic effects.

Also deserving of mention here is the magnetic version of BGK waves with resonant particles becoming magnetically trapped which is observed when the Weibel instability (WI) saturates. Stabilization occurs when the magnetic bounce frequency becomes roughly as large as the linear mode growth rate. Recently, the classic Weibel instability received attention for its applicability in various contemporary problems of laser-plasma interaction as the fast ignitor (see Refs. 5–7) or in the various astrophysical situations as the study of physical processes for generating magnetic fields in gamma ray burst sources (see Refs. 8–13). Plasmas in these astrophysical and cosmic environments are highly energetic and therefore the Weibel instability requires a relativistic treatment. As previously indicated, the theoretical studies of large-amplitude transverse waves include investigations of the quasilinear evolution and nonlinear saturation via magnetic trapping[15] of Weibel instabilities. The system tends to a quasi-steady state which supports a magnetic-type BGK wave. However, previous analytical studies concern the non relativistic regime of the Weibel instability. Analytical studies on the derivation of relativistic Vlasov-Maxwell solutions are still rare. The first theoretical studies of relativistic laser pulses in plasmas date again back to 1950s,[14] when it was recognised that an analytical simplification of coupled relativistic fluid equations is allowed by the introduction of a circularly polarized electromagnetic wave. More recently, relativistic solutions concerning electromagnetic solitons have been published using a kinetic treatment by Lontano *et al.* in Refs. 16 and 17, while later Eliasson and Shukla revisited the concept of relativistic holes in phase space in Ref. 18. In Ref. 17, localized aperiodic stationary solutions have been found in the case of a hot plasma sustaining a relativistically intense soliton-type electromagnetic structure. In the present paper, we revisit the problem of the Weibel instability and its nonlinear saturation via magnetic trapping in the relativistic regime.

Our aim is here to study and characterize the magnetic BGK-type equilibrium, met at saturation of WI, by applying the multistream concept recently proposed in Refs. 19 and 20. The multistream model is a reformulation of the invariance properties of the canonical momentum in the perpendicular direction in the usual reduction techniques used in the Hamiltonian formalism. In Ref. 21, further called Paper I, this formalism was restated to also accommodate the relativistic effects in WI. In Secs. II and III, we focus our attention on the properties of relativistic stationary solutions of the Vlasov-Maxwell system in the presence of magnetic trapping,

which differ here from the relativistic soliton-type solutions predicted by Lontano *et al*. Here, the obtained equilibria can be viewed as the relativistic counterpart of the magnetic BGK modes introduced by Berger and Davidson in Ref. 15. The analytical calculations are checked against numerical simulations of the multistream model, shown in Sec. IV. The coupling with the electrostatic particle trapping is investigated in Sec. V. Our conclusions are presented in Sec. VI. Some auxiliary calculations are also given in Appendix. Results obtained here will also be used in paper III in Ref. 22 where numerical comparisons will be performed to study the saturation regime of WI.

II. BASIC MODEL FOR MAGNETIC BGK WAVES

We start from the work of Lontano *et al*., which has allowed the authors in Refs. 16 and 17 to construct a class of relativistic electromagnetic soliton-type solution of the Maxwell-Vlasov system. In Refs. 16 and 17, the theoretical investigation is based on the use of two key hypotheses: the invariance property of the perpendicular canonical momentum and the introduction of a circular polarization for the electromagnetic field followed the pioneer work of Alkiezer and Polovin in Ref. 14. The authors use the assumption of a cold transverse direction in momentum, while keeping a finite constant parallel temperature. The structure of the equilibrium corresponds to a Dirac-type distribution in the perpendicular momentum direction. Such a hypothesis allows the authors to build a class of exact solutions for describing aperiodic Vlasov-Maxwell equilibria leading to the soliton-like solutions. However, when Weibel-type instabilities are considered, such a hypothesis is no longer valid since we need to introduce a finite perpendicular temperature which makes the calculations more difficult. An alternative is then to consider a multi-stream approach in the perpendicular direction in momentum space which allows to take into account a finite plasma temperature in $\boldsymbol{p}_\perp$. However, the mathematical treatment is here very similar to that used in Refs. 16 and 17 since we use an ensemble of Dirac-type distributions for the different streams or "particle bunches."

By extending the analogy with the Lontano's solution, we may infer further that particle trapping scenario met at saturation of WI, in the relativistic regime, would be similarly described by a nonlinear theory using Dirac distribution in $\boldsymbol{p}_\perp$. We may surmise that similar "BGK-waves" must exist for the plasma in the relativistic regime and we may use our knowledge of the soliton-type solution of Lontano, which exhibits a mixed electromagnetic-electrostatic character to guess the nature of the electromagnetic particle trapping acting as a saturation process for WI. Finally, one might also expect that, in the limit of weak magnetic fields, the self-consistent solution of the reduced Vlasov-Maxwell system (here described by the multistream model) would correspond to a dominant magnetic particle trapping version, at least in the case of a circularly polarized potential vector. In the general case and for a linearly polarized electromagnetic field, particles experience a mixed electrostatic and magnetic trapping. This inference would be confirmed later directly by numerical simulations based from the multistream model, both in the strongly nonlinear and relativistic regimes.

Following the approach of Akhiezer and Polovin in Ref. 14 or that of Berger and Davidson in Ref. 15, the research of a stationary solution is thus facilitated by the introduction of a circularly polarized potential vector in the form

$$\boldsymbol{A}_\perp(x,t) = A_0\cos(k_0x)\boldsymbol{e}_y + A_0\sin(k_0x)\boldsymbol{e}_z. \tag{1}$$

Therefore, it is then possible to introduce the concept of "ring" and to allocate the different streams on a circular ring of constant radius $C_{\perp j}$ as previously proposed in Part I companion paper in Ref. 21. Thus, without loss of generality, for a class of exact solutions of streams having a canonical momentum

$$\boldsymbol{C}_j = C_{\perp j}\cos\theta_j\boldsymbol{e}_y + C_{\perp j}\sin\theta_j\boldsymbol{e}_z \tag{2}$$

we can introduce random phases θ_j which determine the position of streams on the considered "ring." In order to fix the basic ideas, we first consider the one-ring case and take $N_s = N$ streams (for $j = 1,...,N$) distributed on a circular ring of radius $C_\perp$ in a random way. Notice that $C_{\perp j} = C_\perp$ for $j = 1,...,N$ while keeping the central stream (here denoted by $j = 0$) at the origin in the momentum space. For this central stream, we have indeed $C_{\perp 0} = 0$ and we may consider this system as a two-ring case for which the central ring is a Dirac-type distribution—i.e., a stream- of zero radius.

Here, we choose to solve a system of several Vlasov-type equations in the multistream approach rather than the one-dimensional 1D3V Vlasov equation, which is frequently considered in other works. Thus, in the multi-stream approach, we have to solve $N+1$ reduced Vlasov-type equations, which can be written in the form (for $0 \le j \le N$)

$$\frac{\partial f_j}{\partial t} + \frac{p_x}{m\gamma_j}\frac{\partial f_j}{\partial x} - \frac{\partial}{\partial x}(mc^2\gamma_j + e\phi)\frac{\partial f_j}{\partial p_x} = 0. \tag{3}$$

The stationary solution ($\partial/\partial t = 0$) of Eq. (3) is any function $F_j(\varepsilon_j)$ of the total relativistic energy $\varepsilon_j = mc^2\gamma_j + e\phi$ for the particle stream noted j and the dependence on the variable C_j is made through the Lorentz factor γ_j given by $\gamma_j^2 = 1 + \frac{p_x^2}{m^2c^2} + \frac{(\boldsymbol{C}_j - e\boldsymbol{A}_\perp)^2}{m^2c^2}$. The structure of the electron distribution function can now be taken as a multistream-type and the particle distribution, for the jth stream, writes in the form of a Maxwell-Boltzmann-Jüttner distribution

$$f_j(x,p_x) = S_j\exp(-\mu\gamma_j)\exp\left(-\mu\frac{e\phi}{mc^2}\right), \tag{4}$$

where $\mu = \frac{mc^2}{T_\parallel}$ is the relativistic factor which determines the features on temperature in the longitudinal direction in p_x. Here, the quantity S_j is a constant of normalization. By integrating (4) over p_x, it is easy to calculate the density of the jth stream, so one obtains

$$n_j(x) = S_j\exp\left(-\mu\frac{e\phi}{mc^2}\right)2mc\sqrt{1+U_j^2(x)}K_1\left(\mu\sqrt{1+U_j^2(x)}\right), \tag{5}$$

where we have introduced the quantity U_j^2 defined by

$$U_j^2(x) = \frac{(\boldsymbol{C}_j - e\boldsymbol{A}_\perp).(\boldsymbol{C}_j - e\boldsymbol{A}_\perp)}{m^2c^2}. \tag{6}$$

In addition to n_j that we presented, we can also define the perpendicular component of the current density, for the jth stream. In a similar way, one gets

$$\boldsymbol{J}_{\perp j} = 2mcS_j\frac{e}{m}(\boldsymbol{C}_j - e\boldsymbol{A}_\perp)\exp\left(-\mu\frac{e\phi}{mc^2}\right)K_0\left(\mu\sqrt{1+U_j^2(x)}\right), \tag{7}$$

where K_n is the modified Bessel function of second kind and of order n. Using the expressions of the potential vector $\boldsymbol{A}_\perp$, in a circular polarization and of the canonical momentum given by Eqs. (1) and (2), respectively, the function $U_j^2(x)$ rewrites as follows:

$$U_j^2(x) = a_0^2 + \frac{C_{\perp j}^2}{m^2c^2} - \frac{2C_{\perp j}a_0}{mc}\cos(k_0x - \theta_j) \tag{8}$$

with the standard normalized potential vector amplitude of $a_0 = \frac{eA_0}{mc}$. From the normalization condition on f_j for the jth stream, which writes as $\int_0^L \frac{dx}{L}\int_{-\infty}^{+\infty} dp_x f_j(x,p_x,t) = n_0\alpha_j$ (and where the summation over the different beam densities is taken to one), it can be easily verified that the normalized factor S_j reads as

$$S_j = \frac{n_0\alpha_j}{D_j} = \frac{n_0\alpha_j}{\int_0^L \frac{dx}{L}\exp\left(-\mu\frac{e\phi}{mc^2}\right)2mc\sqrt{1+U_j^2(x)}K_1\left(\mu\sqrt{1+U_j^2(x)}\right)}. \tag{9}$$

Using the density n_j and the corresponding current density $\boldsymbol{J}_{\perp j}$, associated to the stream j, defined by Eqs. (5) and (7), respectively. Equations for the potential vector $\boldsymbol{A}_\perp$ and the electric potential write now, respectively

$$\frac{\partial^2\boldsymbol{A}_\perp}{\partial t^2} - c^2\frac{\partial^2\boldsymbol{A}_\perp}{\partial x^2} + \omega_p^2 e^{-\mu\frac{e\phi}{mc^2}}\sum_{j=0}^{N}\frac{2mc\alpha_j}{D_j}K_0\left(\mu\sqrt{1+U_j^2(x)}\right)\boldsymbol{A}_\perp = \frac{\omega_p^2}{e}e^{-\mu\frac{e\phi}{mc^2}}\sum_{j=0}^{N}\frac{\alpha_j\boldsymbol{C}_j}{D_j}K_0\left(\mu\sqrt{1+U_j^2(x)}\right), \tag{10}$$

$$\frac{d^2\phi}{dx^2} = \frac{n_0e}{\epsilon_0}\left[1 - e^{-\mu\frac{e\phi}{mc^2}}\sum_{j=0}^{N}\frac{2mc\alpha_j}{D_j} \times\sqrt{1+U_j^2(x)}K_1\left(\mu\sqrt{1+U_j^2(x)}\right)\right]. \tag{11}$$

Therefore, we are faced with the mathematical problem of solutions of a coupled nonlinear system of two second order differential equations given by Eqs. (10) and (11), depending on the physical parameters $\{\mu, \alpha_j, C_{\perp j}, \theta_j\}$. They can be put into a Hamiltonian form, using a procedure similar to the one employed by Lontano *et al.* in Refs. 16 and 17 or by Haas *et al.* in Ref. 23 in the case of the study of quantum plasmas using a multistream model. Equations (10) and (11) constitute a closed set of one-dimensional relativistic equations for the potential fields ϕ and $\boldsymbol{A}_\perp$, interacting with a hot plasma, whose macroscopic state has been consistently derived from the stationary solution given in Eq. (4) of the reduced Vlasov equations (3). While the set of Eqs. (10) and (11) admits an aperiodic solution in the case of a single stream, it is however possible to build a periodic (BGK-type) solution when several streams are considered, allowing to take into account a finite perpendicular temperature.

III. MAGNETIC BGK WAVE IN THE LIMIT OF WEAK FIELDS

It is then instructive to examine the structure of the stationary solution of the set of Eqs. (3), (10), and (11) in the limit of weak fields or when strong perpendicular temperature is considered. It follows that we can now assume that $a_0 \ll \frac{C_\perp}{mc}$ and the quantity $\sqrt{1+U_j^2(x)}$ can be approximated. To simplify the presentation, we assume also that $\phi \to 0$. In the general case, the electric potential can be chosen to be as small as possible in the case of a circularly polarized potential vector at least in the limit where the amplitude of the potential vector is weak.

At this step, we introduce normalized quantities as $\boldsymbol{a}_\perp = \frac{e\boldsymbol{A}_\perp(x,t)}{mc}$, the spatial x and time t coordinates become now dimensionless quantities, respectively, normalized to $d_e = c\omega_p^{-1}$ and to ω_p^{-1}. One gets

$$\sqrt{1+U_j^2(x)} \simeq \sqrt{1+a_0^2+C_{\perp j}^2} - \boldsymbol{a}_\perp.\boldsymbol{C}_j = \sqrt{1+a_0^2+C_{\perp j}^2} - a_0C_{\perp j}\cos(k_0x - \theta_j), \tag{12}$$

where the vector $\boldsymbol{C}_j$, of modulus $C_{\perp j}$, is now normalized to mc. By using Eq. (12), one can express the modified Bessel function K_n of argument $\mu\sqrt{1+U_j^2(x)}$ in terms of $z_j = \mu\sqrt{1+a_0^2+C_{\perp j}^2}$ and $\boldsymbol{a}_\perp.\boldsymbol{C}_j$ as

$$K_n\left(\mu\sqrt{1+U_j^2(x)}\right) \simeq K_n(z_j) - \boldsymbol{a}_\perp.\boldsymbol{C}_j\frac{dK_n}{dz}(z_j). \tag{13}$$

In dimensionless quantities, it is possible to write the equation for $\boldsymbol{a}_\perp$ which becomes, to the first order in $\boldsymbol{a}_\perp.\boldsymbol{C}_j$, and by using for the first derivative of $\frac{dK_0}{dz} = -K_1(z)$

$$\frac{\partial^2\boldsymbol{a}_\perp}{\partial t^2} - \frac{\partial^2\boldsymbol{a}_\perp}{\partial x^2} + \boldsymbol{a}_\perp\sum_{j=0}^{N}\frac{\alpha_j}{D_j}[K_0(z_j) + \mu\boldsymbol{a}_\perp.\boldsymbol{C}_jK_1(z_j)] = \sum_{j=0}^{N}\frac{\alpha_j\boldsymbol{C}_j}{D_j}[K_0(z_j) + \mu\boldsymbol{a}_\perp.\boldsymbol{C}_jK_1(z_j)]. \tag{14}$$

We can now perform an average over the random phase θ_j of the streams distributed on the ring of radius $C_{\perp j} = C_\perp$ for $1 \le j \le N$ (included in the term $\boldsymbol{a}_\perp.\boldsymbol{C}_j$). Notice that for the

central stream, i.e., $j=0$, the corresponding value is $C_{\perp 0}=0$. This average operator will be used to eliminate all terms of first order in $\boldsymbol{a}_\perp.\boldsymbol{C}_j$ except the contribution in $(\boldsymbol{a}_\perp.\boldsymbol{C}_j)\boldsymbol{C}_j$ in the right-hand member in Eq. (14).

Assuming that the streams are distributed in a random way on a given ring and the mean value of $\langle \boldsymbol{C}_j\rangle_{\theta_j}\to 0$, allowing to suppress the contribution of the $(\boldsymbol{a}_\perp.\boldsymbol{C}_j)\boldsymbol{a}_\perp$ non linear term in Eq. (14), one gets

$$\frac{\partial^2 \boldsymbol{a}_\perp}{\partial t^2}-\frac{\partial^2 \boldsymbol{a}_\perp}{\partial x^2}+\sum_{j=0}^{N}\frac{\alpha_j}{D_j}K_0(z_j)\boldsymbol{a}_\perp=\sum_{j=0}^{N}\frac{\alpha_j}{D_j}\mu\langle \boldsymbol{C}_j(\boldsymbol{a}_\perp.\boldsymbol{C}_j)\rangle_{\theta_j}K_1(z_j). \tag{15}$$

By replacing now the expression of $D_j=\sqrt{1+a_0^2+C_{\perp j}^2}$ $K_1(z_j)$ in Eq. (15) and keeping the nonlinear contribution in $\boldsymbol{C}_j$, we remain with a single linearized equation for $\boldsymbol{a}_\perp$ in the form

$$\frac{\partial^2 \boldsymbol{a}_\perp}{\partial t^2}-\frac{\partial^2 \boldsymbol{a}_\perp}{\partial x^2}+\sum_{j=0}^{N}\alpha_j\mu\frac{K_0(z_j)}{z_jK_1(z_j)}\boldsymbol{a}_\perp=\sum_{j=0}^{N}\frac{\alpha_j}{z_j}\mu^2\langle \boldsymbol{C}_j(\boldsymbol{a}_\perp.\boldsymbol{C}_j)\rangle_{\theta_j}. \tag{16}$$

Several remarks must be pointed out:

(i) First, it can be easily verified that the case where $\boldsymbol{C}_j=0$ in Eq. (16) cannot sustain periodic BGK-type solutions. We indeed recover the standard dispersion relation of propagating electromagnetic waves in plasma which reads in normalized quantities as $\omega^2=k^2+\sum_{j=0}^{N}\mu\alpha_j\frac{K_0(z_j)}{z_jK_1(z_j)}$.

(ii) More generally, in the case of WI, dropping now the time derivative $(\frac{\partial}{\partial t}=0)$ in the linear version of the potential vector equation in Eq. (16) (but keeping the nonlinear contribution in $\boldsymbol{C}_j$), we seek steady-state solutions of Eq. (16) for the case where the right-hand side in Eq. (16) is now different of zero. By replacing the averaged term $\langle \boldsymbol{C}_j(\boldsymbol{a}_\perp.\boldsymbol{C}_j)\rangle_{\theta_j}$ by its value $0.5C_{\perp j}^2\boldsymbol{a}_\perp$, Eq. (16) reads now

$$\frac{d^2 \boldsymbol{a}_\perp}{dx^2}+\left[\sum_{j=0}^{N}\frac{\alpha_j\mu^2C_{\perp j}^2}{2z_j}-\sum_{j=0}^{N}\frac{\alpha_j\mu K_0(z_j)}{z_jK_1(z_j)}\right]\boldsymbol{a}_\perp=0. \tag{17}$$

Substituting Eq. (1) into Eq. (17) determines k_0 self-consistently in the dimensionless form (with $z_j=\mu\sqrt{1+a_0^2+C_{\perp j}^2}$)

$$k_0^2=\sum_{j=0}^{N}\frac{\alpha_j\mu^2C_{\perp j}^2}{2z_j}-\sum_{j=0}^{N}\frac{\alpha_j\mu K_0(z_j)}{z_jK_1(z_j)}. \tag{18}$$

In Eq. (18), k_0^2 can take a positive value provided that $\sum_{j=0}^{N}\frac{\alpha_j\mu^2C_{\perp j}^2}{2z_j}>\sum_{j=0}^{N}\frac{\alpha_j\mu K_0(z_j)}{z_jK_1(z_j)}$. As a specific example, consider the Yoon's and Davidson's solution for a single ring without central beam, i.e., for $\alpha_0=0$ and $\sum_{j=1}^{N}\alpha_j=1$. Therefore, we have (using $z=\mu\sqrt{1+a_0^2+C_\perp^2}$)

$$k_0^2=\mu\left(\frac{C_\perp^2}{2\sqrt{1+a_0^2+C_\perp^2}}-\frac{K_0(z)}{zK_1(z)}\right)>0 \tag{19}$$

provided that we take $C_\perp$ sufficiently large, or equivalently, by considering large relativistic perpendicular temperature $(C_\perp\geq 2.5)$. In fact, for $0.5\leq z\leq 5$, the function $K_0(z)/zK_1(z)$ decreases from 1.116 to 0.189.

To summarize periodic stationary solutions may be found after applying the Hamiltonian reduction technique to the Vlasov-Maxwell model, when a single ring is introduced in the transverse direction in momentum space, in addition to the central Dirac-type stream. For a given stream, localized on the ring, particles experience their own magnetic bounce frequency which, from Eq. (A10) in Appendix, can be written, for a deeply trapped particle population as

$$\omega_{bj}^2=\frac{k_0^2C_{\perp j}a_0}{\gamma_{0j}^2}. \tag{20}$$

Here, γ_{0j} is given by the Lorentz factor $\sqrt{1+a_0^2+C_{\perp j}^2}$ in normalized units (see Appendix). Notice that, from Eq. (16), the periodic solution breaks down, when the second member of Eq. (16) disappears, showing the key role played by the contribution of the $C_\perp^2$ term. Because the magnetic-type BGK waves arise naturally in the asymptotic behaviour of Weibel instabilities (as we will see in future section and in Paper III), the Hamiltonian multistream model can be used to obtain an accurate description of complex phenomena met in WI at saturation.

IV. NUMERICAL SIMULATIONS AFFORDED BY THE MULTISTREAM MODEL

In our simulations, we make use of a kinetic and full relativistic semi-lagrangian solver[24,25] which solves the Vlasov equation by direct discretization of the phase space. Such a code displays a very low noise level, even in zones of low density and is thus to be preferred to usual particle-in-cell (PIC) codes. Our numerical model solves the Vlasov equations (3) for each stream j coupled with the Maxwell equations for fields in a self-consistent way. In this section, we present first results from the multistream Vlasov simulations to investigate the key role played by the magnetic trapping during the saturation regime of WI and the stability of the resulting magnetic BGK structures occurring in phase space.

The mechanism of WI depends on the free energy which is stored in an anisotropy particle distribution in momentum space. For relativistic plasmas, the most common distribution function is the Maxwell-Jüttner distribution. There is an extensive literature relating to dispersion in finite temperature, especially relativistic and thermal plasmas. While Saheer et Murtaza introduced a semirelativistic Maxwellian distribution in Ref. 26 to investigate WI, the Yoon's model[27,28] represents the first attempt to generalize the Maxwell-Jüttner distribution to include temperature anisotropy in the relativistic regime. More recently, Schlickeiser introduced a newly bi-Maxwellian distribution from covariant approach of dispersion theory of linear waves in Ref. 29. To show the possibilities of our multistream approach, we

adopt to characterize the temperature anisotropy using the normalized distribution function of Schlickeiser while keeping a Dirac comb in $\boldsymbol{p}_\perp$. Thus, at the equilibrium, the distribution reads

$$F_0(p_x,\boldsymbol{p}_\perp,t=0)=\sum_{j=0}^{N}\alpha_j e^{-\mu\sqrt{1+p_x^2+\boldsymbol{p}_\perp^2}-\mu\psi p_x^2}\delta(\boldsymbol{p}_\perp-\boldsymbol{C}_j), \tag{21}$$

where the different streams, except the case of the "central" beam, are distributed over a single circular "ring" in the perpendicular momentum space $\boldsymbol{p}_\perp$ of radius chosen here as $C_{\perp j}=p_{\perp th}$ for every value of j taken between 1 and N, and where $p_{\perp th}$ denotes the thermal momentum in the perpendicular direction approximated by $\frac{p_{\perp th}^2}{2\sqrt{1+p_{th,\perp}^2}}=\frac{1}{\mu}=\frac{T_\perp}{mc^2}$. For each stream j, the density is α_j given by $\alpha_j=\frac{1-\alpha_0}{N}$. For the central stream, the density corresponds to α_0 and we take $C_{\perp 0}=0$. Here, the normalization condition for F_0 writes $\sum_{j=0}^{N}\alpha_j=1$ and the coefficients α_j are calculated numerically from the data of the Schlickeiser's distribution. Notice that the temperature anisotropy is described by the factor ψ taken close to 4 and we have checked that no instability arises when $\psi=0$. The distribution function is then perturbed by magnetic fluctuations on the components of the magnetic field by using

$$\delta\boldsymbol{B}=\sum_{m=1}^{M}b_0\cos\left(\frac{2\pi mx}{L}+\nu_m\right)\boldsymbol{e}_y+\sum_{m=1}^{M}b_0\sin\left(\frac{2\pi mx}{L}+\nu_m\right)\boldsymbol{e}_z, \tag{22}$$

where ν_m are random phases and $b_0=10^{-5}$ is the normalized mode amplitude. We have taken $M=20$ modes and a plasma length of $L=16\pi d_e$. Finally, ions were taken to form an infinitely massive uniform background. This is a valid approximation since, for realistic ion masses, the ion motion would not participate in the instability on the time scale of interest.

A first numerical simulation was performed using a phase space sampling of $N_xN_{p_x}=1024\times 513$ while the typical time step is $\Delta t=0.025$. Together with the central beam located at $C_{\perp 0}=0$, of density $\alpha_0\simeq 0.217$, we have introduced $N=8$ streams, of same density $\alpha_j=\frac{1-\alpha_0}{N}\simeq 0.0978$, distributed in random way on a single "ring." We choose here to take $C_\perp=p_{th,\perp}\simeq 2.40mc$ which corresponds to $T_\perp\simeq 570\,\mathrm{keV}$ while the parallel temperature is close to $T_\parallel=\frac{T_\perp}{2\psi+1}\simeq 60\,\mathrm{keV}$.

Fig. 1 exhibits the time evolution of the magnetic energy for the dominant Fourier mode $m=3$ in a logarithmic scale. WI proceeds through the linear stage (for $0\le t\omega_p\le 40$), in which the magnetic field strength grows exponentially in time, followed by the nonlinear saturation stage, in which magnetic trapping is expected. Here, the numerical growth rate of WI is found close to $\Gamma_{num}\simeq 0.23$. The corresponding time evolution of the mode $m=3$ of the inductive part of the electric field E_y is shown on top panel in Fig. 2, showing a strong decrease of the electric energy when the instability saturates. A similar behaviour is observed for the y-component of $\boldsymbol{E}$ indicating that the vector potential $\boldsymbol{A}_\perp$ (linked to the field $\boldsymbol{E}_\perp$ through the relation $\boldsymbol{E}_\perp=-\frac{\partial\boldsymbol{A}_\perp}{\partial t}$) tends to a quasi-stationary solution. In order to completely figure out the electric energy of the system, one must also consider the electrostatic contribution due to the x-component of the electric field. The time evolution of the normalized quantity E_x is

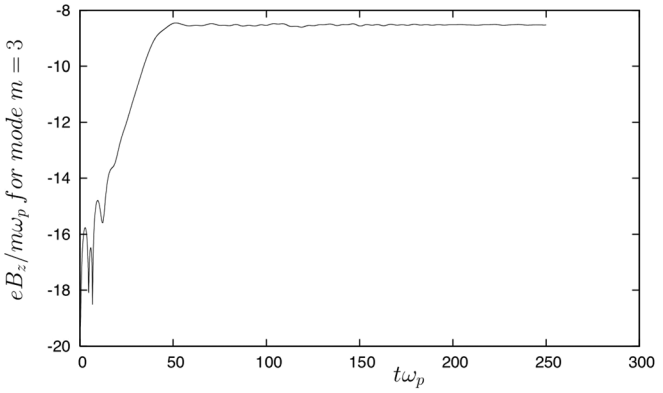

FIG. 1. Time evolution of the magnetic energy for the dominant Fourier mode $m=3$ in a logarithmic scale. WI proceeds through the linear stage for $t\omega_p\le 40$, in which the magnetic field strength grows exponentially in time, followed by the nonlinear saturation stage where magnetic trapping takes place.

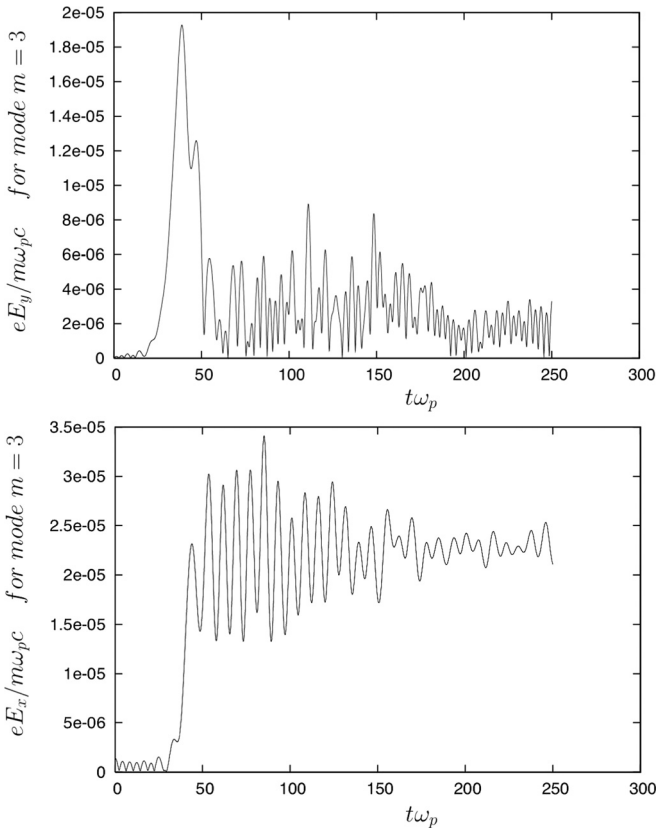

FIG. 2. On top panel: Corresponding time evolution of the mode $m=3$ of the inductive part of the electric field E_y showing a strong decrease of the electric energy when the instability saturates. On bottom panel: corresponding electrostatic part E_x showing that the field is non negligible at the saturation. Thus, the mode $m=3$ results from the mixture of both magnetic and electrostatic contributions. The perpendicular temperature is here $T_\perp\simeq 570\,\mathrm{keV}$ and we have used $\psi=4$.

thus plotted on the bottom panel in Fig. 2. It should be noticed that the growth is delayed in comparison with that of E_y but reaches a high level of saturation. The study of the long-term evolution of E_x in the system shows, that after a stage during which the field grows, due to nonlinear coupling, the evolution goes on, until the field starts to oscillate at a high frequency value close to $\omega \simeq 0.80$. Note that one can estimate the square of the relativistic plasma frequency by the relation

$$\bar{\omega}_p^2 = \sum_{j=0}^{N} \frac{\alpha_j}{\gamma_{0j}} \simeq 0.48 \tag{23}$$

i.e., the electric field oscillates at a frequency somewhat higher than $\bar{\omega}_p \simeq 0.70$ in ω_p-units. This behaviour of E_x immediately points out a feature that distinguishes the asymptotic solution seen in the simulation from the purely magnetic BGK solution studied previously in the limit of weak fields. Now the dominant mode $m = 3$ is a mixture of longitudinal and transverse fields due to the nonlinear coupling induced by the $A_\perp^2$-terms. In these conditions, to obtain an electrostatic field E_x so strong, we expect that the particles resonate with the plasma frequency leading to growth of a longitudinal plasma wave which can also contribute to the particle trapping. However, the dominant trapping mechanism seems to be the magnetic trapping, at least at the beginning of the saturation mechanism.

The multistream model allows us to separate the dynamics of streams and focus on the time evolution of a distribution function $f_j(x, p_x, t)$ in phase space. The most striking advantage of this model is the very fine resolution in phase space capable of resolving the finest mechanism of particle trapping. This is because, our model renders possible a detailed examination of the low density regions of the phase space, especially the description of the tail phenomena, where only a small number of particles is involved and where particle trapping occurs. The impact of the magnetic trapping on the distribution function shape is shown in Fig. 3 where we have displayed the $x - p_x$ phase space for a stream chosen among the different streams located on the circular ring. We show the shaded iso-contours of one of the streams located on the ring of momentum $C_\perp = 2.42mc$. The case of the central beam located at the origin of the perpendicular momentum space is shown in Fig. 4.

In Fig. 3, we observe the formation of three vortex-type structures, not in phase, due to the initial fluctuations on the magnetic field, exhibiting a perturbation made on several modes. Owing to the very good resolution in phase space afforded by our Vlasov code, one can begin to understand much of the details of the saturation process. The asymptotic behaviour of the stream particle population is shown on bottom panel in Fig. 3. The numerical model implies necessarily a discretization of phase space, which can create a "cleaning" in the temporal evolution of the fine structure developed by the Vlasov equation. When the filamentation in momentum space reaches the size of the elementary cell $\Delta x \Delta p_x$, the treatment of the information is not exactly effected, leading to the phenomenon of "cleaning" of the distribution in phase space. We see clearly on the two first pictures of Fig. 3 the formation

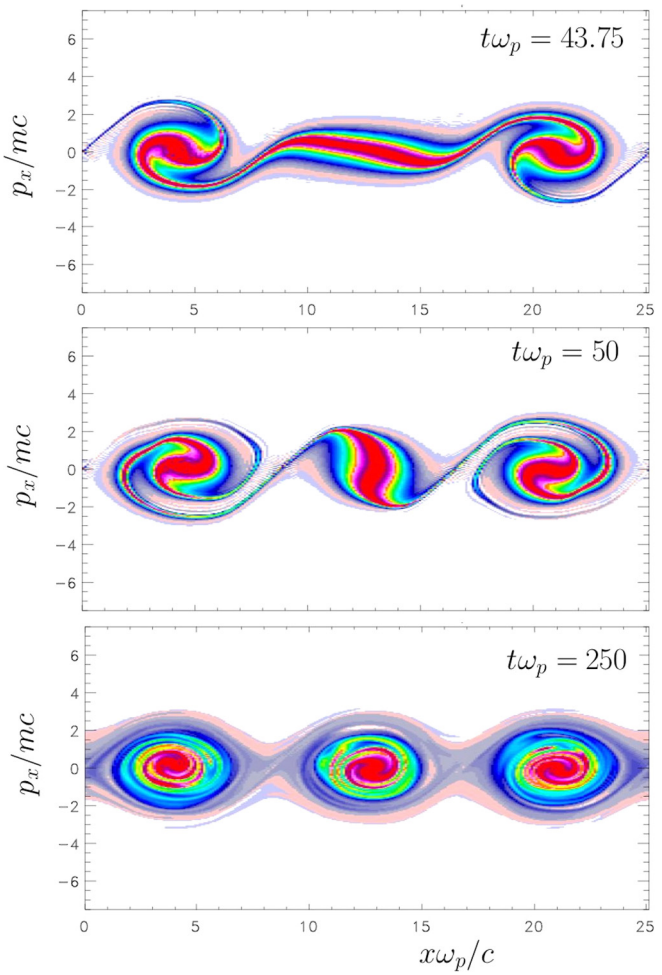

FIG. 3. Phase space representation of a selected "stream" of the ring in the $x - p_x$ phase space. The distribution of the trapped particle population exhibits a three-vortex structure as the result of the magnetic trapping. The perpendicular temperature is here $T_\perp \simeq 570\,\text{keV}$ and we have used $\psi = 4$.

of the vortices with a filamentary structure rotating around the vortex. Then the "cleaning" takes place, filling the gaps between the filaments, destroying consequently the mathematical topology properties of the Vlasov equation (the vacuum region of the vortex must be continuously connected to the external $\frac{p_x}{mc} \geq 12$ vacuum region), but in a certain sense, restoring the physical properties of the plasma, since we must remember that the Vlasov equation model is an asymptotic one whose diffusion process in velocity space (or in momentum space here) has been neglected. However, this numerical diffusion does not affect here the behaviour of the plasma provided that the phase space sampling is sufficient. Thus after $t\omega_p = 150$, the apparent vortex structure in the plasma evolves any more and we obtain a stationary state at $t\omega_p = 250$. The formation of the vortices corresponds to the presence of a small population of trapped particles, but which play a fundamental role in the stopping of the growth of the Weibel instability.

Of course certain specific aspects of the instability are here lost because we have only used one ring in the perpendicular space; however, general features induced by magnetic trapping can be recovered when a single ring is used. The behaviour of the different streams of a same ring is

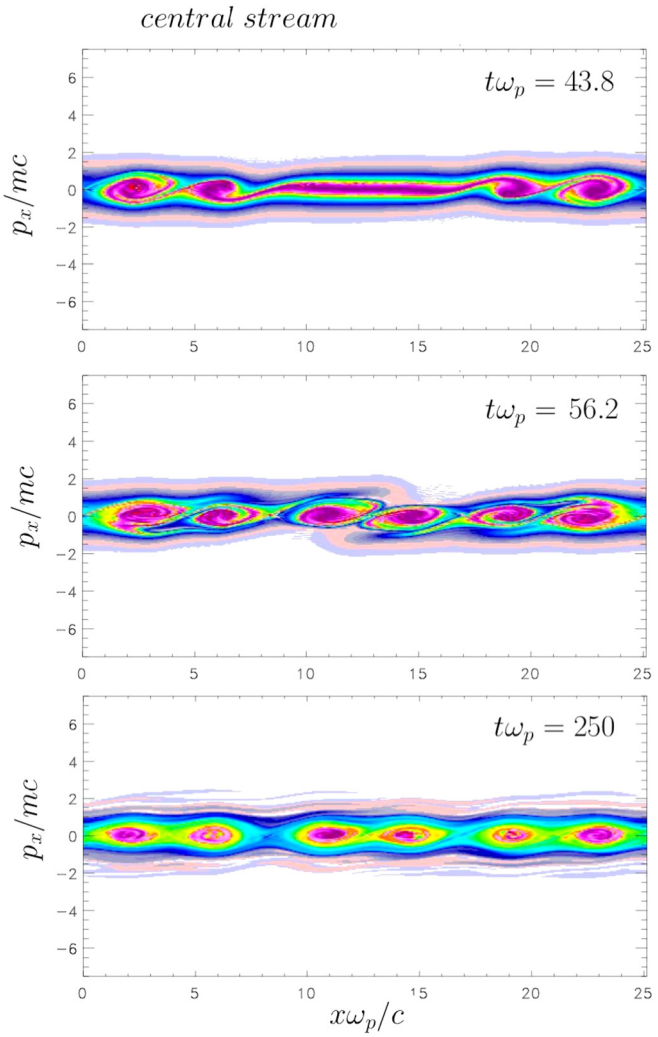

FIG. 4. Representation of the central stream in phase space for the same system shown in Fig. 3. We can see clearly the formation and the growth of vortices induced by the presence of both modes $m=3$ (i.e., the mode k_0) and $m=6$ (the harmonic $2k_0$). Notice that the plasma "heating" is weaker for the plasma bulk. Numerical results correspond to $T_\perp \simeq 570\,\mathrm{keV}$ and to an anisotropy factor of $\psi = 4$.

slightly different due to the effects generated by the random phases introduced initially. The streams experience a magnetic effective potential energy $\boldsymbol{a}_\perp.\boldsymbol{C}_j$ (see Eq. (12)) or equivalently $a_0 C_{\perp j}\cos(k_0 x - \theta_j)$ depending of the random phase θ_j.

In many aspects, the results presented here confirm the key role played by the magnetic trapping. It was also found that the electric field is very weak compared to the magnetic field. Although they are a minority in number, these trapped particles of the ring contribute significantly to the saturation process (it is not the case of particle population of the central beam as we will see later). On the other hand, there is a striking difference between the time evolution for particles of the central beam and those for the ring. Fig. 4 shows a representation of the distribution of the central stream in phase space. From Fig. 4, it is clear that nonlinear effects induced by the Lorentz force, i.e., the $\boldsymbol{a}_\perp^2$-term are here important. Fig. 4 shows clearly the formation and the growth of vortices induced by the presence of both modes $m=3$ (i.e., the mode k_0) and $m=6$ (the harmonic $2k_0$). Note that, for the central stream, the magnetic bounce frequency tends to zero since $C_{\perp 0}=0$. We found that strong magnetic trapping effects occur only for the particle population of streams of the ring and that the size of the magnetic vortices, in momentum, is bigger in comparison with that of the phase space vortices observed in the central stream, which are indeed induced by the "electrostatic" contribution.

The vortices associated to the growing mode $m=6$, clearly visible at the beginning at $t=56.2$, start to pair eventually (however without reaching the coalescence) leading to three global structures, each structure being formed by two smaller vortices. For a deeply trapped particle population of the ring, a value of the magnetic bounce frequency, in the relativistic regime, is given by Eq. (20) which becomes in normalized units

$$\omega_B = \sqrt{k_0 \frac{C_\perp}{\gamma_\perp}\omega_{ce}}, \tag{24}$$

where $\omega_{ce} = \frac{B_{max}}{\gamma_\perp}$ is the electron cyclotron frequency (normalized to ω_p). By introducing standard normalization units, we have then $C_\perp \simeq 2.40$ and the corresponding Lorentz factor is close to $\gamma_\perp = \sqrt{1+a_0^2+C_\perp^2} \simeq 2.67$ for a value of $a_0 = B_{max}/k_0 = 0.40/0.75 = 0.533$. We obtain a corresponding estimate of the magnetic bounce frequency for a stream of the ring close to $\omega_B \simeq 0.32$, i.e., a value somewhat higher than the linear growth rate of $\Gamma = 0.23$. In the multistream representation, a physical picture emerges: it is possible to represent the "quasi-linear" version of the magnetic bounce frequency as a mean frequency $\bar{\omega}_B$ seen by the different particle stream populations. Thus, $\bar{\omega}_B$ can be defined by the following relation:

$$\bar{\omega}_B = \sum_{j=0}^{N} \alpha_j \omega_{bj} = (1-\alpha_0)\omega_B, \tag{25}$$

where $\alpha_j \simeq 0.0978$ is the beam density for a given stream located on the ring, while the density of the central stream is here $\alpha_0 \simeq 0.217$. Note that $\sum_{j=0}^{N}\alpha_j = 1$ is the normalization condition. Thus, we obtain $\bar{\omega}_B = (1-\alpha_0)\omega_B \simeq 0.249$ in well agreement with the linear growth rate of WI observed in Fig. 1.

V. ROLE OF THE ELECTROSTATIC TRAPPING AND STABILITY

In previous sections, the magnetic trapping is shown to produce a topologically symmetric structure of the distribution function in the stationary state, in the form of a chain of magnetic vortices on the mode k_0, coupled with a chain of electrostatic vortices on the mode twice of k_0. For the better understanding of the nature of phase space structures observed in the central stream, governed by the electrostatic trapping of resonant electrons, we now perform the same simulation by increasing the perpendicular temperature till a value of $T_\perp \simeq 840\,\mathrm{keV}$ (i.e., $p_{th,\perp} \simeq 3.40mc$) while $T_\parallel = \frac{T_\perp}{1+2\psi} \simeq 90\,\mathrm{keV}$ corresponding to an anisotropy factor of $\psi = 4$, and keeping the other physical parameters identical. While allowing now the possibility of coupling between both

kinds of particle trappings, the multistream model offers also the interpretation of structures observed in the central stream and describes also new mechanisms associated with resonant particles, such as pair wise magnetic vortex merging observed in all streams. It will be shown below that the magnetically trapped particles of streams located on the ring also undergo the effects of the electrostatic trapping. In fact, electrostatic trapping is clearly observed in the central stream for which the magnetic bounce frequency vanishes, we can further distinguish two subclasses of trapped particles, the electrostatically and magnetically trapped ones.

Fig. 5 shows the time history of the mode $m=2$ for the magnetic field B_z component, and of the electric field E_x, in normalized units, respectively, on the top and bottom panels. The evolution of the magnetic field is plotted in a logarithmic scale. For the simulation shown in Fig. 5, magnetic fluctuations are introduced on the mode $m=1$ till $m=20$ using a small amplitude of $b_0 = 10^{-5}$ to assure a low initial level of magnetic field fluctuations. The mode $m=2$ is observed to be the dominant mode although another modes are also excited to a weaker levels. For the parameters used in the simulation of Fig. 5, we find from Eq. (25) that $\bar{\omega}_B \simeq 0.21$ in ω_p units using the relation (24) for ω_B and the values of $k_0 = 0.50$ (i.e., the mode $m=2$ here), $B_{max} \simeq 0.60$ and $\gamma_\perp \simeq 3.77$ in normalized units. The numerical growth rate is close to $\Gamma_{num} = 0.20$.

We discuss at first, the behaviour of a ring's stream during the evolution process. The stream is plotted in Fig. 6 at

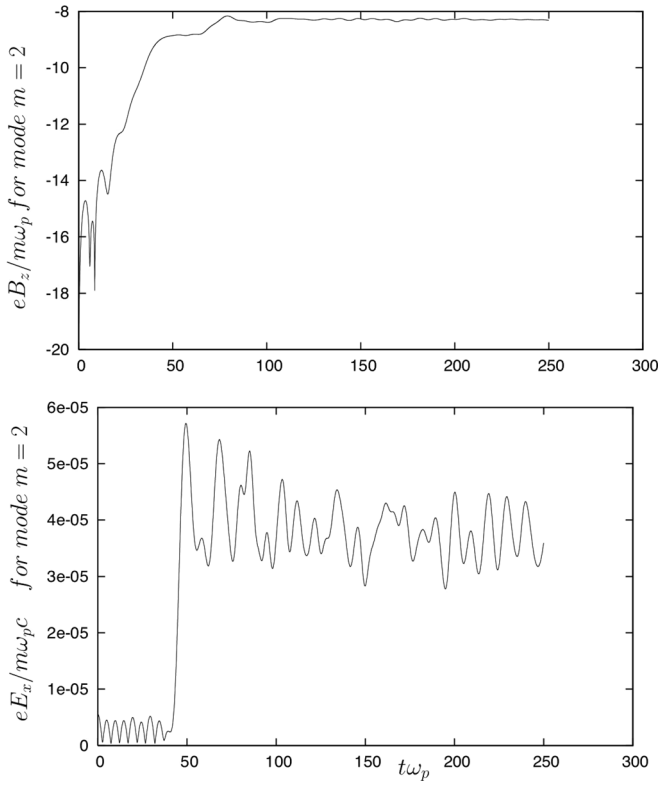

FIG. 5. Time history of the mode $m=2$ for the magnetic field B_z component on top panel, and of the electric field E_x on bottom panel. The evolution of the magnetic field is plotted in a logarithmic scale. The simulation was performed for a higher value of the perpendicular temperature of $T_\perp \simeq 840\,\text{keV}$ using an anisotropy factor of $\psi = 4$.

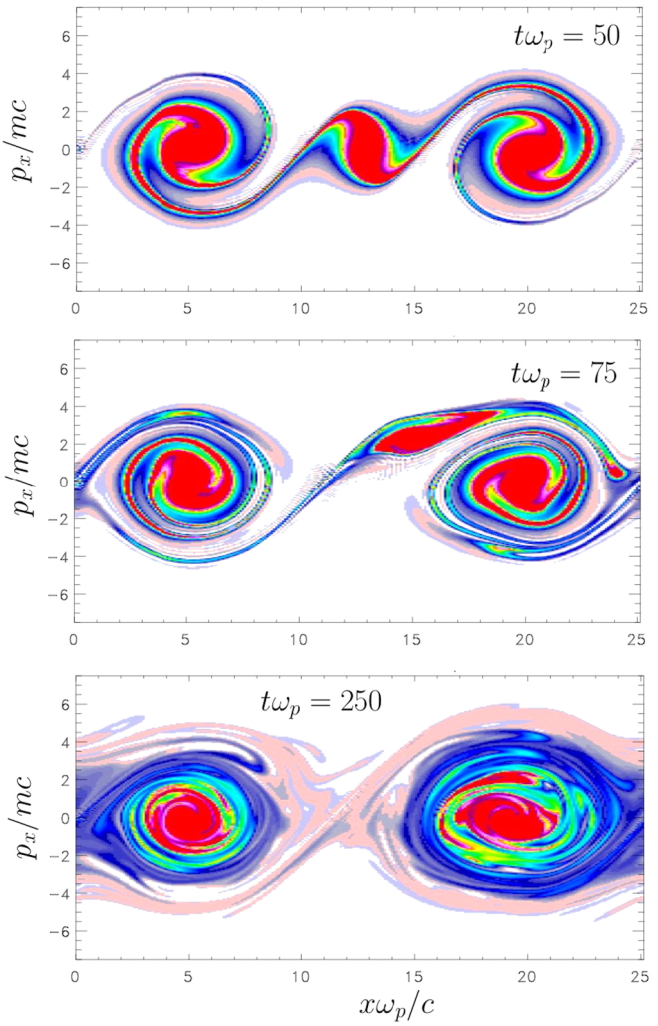

FIG. 6. Plots of the electron distribution function in the phase space for a selected stream of ring. We see clearly the formation of a three-vortex structure on the middle panel, emerging for the growth of the most unstable mode $m=3$. The phase space structure is however unstable and the coalescence of two vortices takes place at time $t=75$ on bottom panel. The perpendicular temperature is here $T_\perp \simeq 840\,\text{keV}$ and we have used $\psi = 4$.

three different times. The top panel in Fig. 6 shows the beginning of the saturation mechanism indicating the presence of both modes $m=2$ and $m=3$. We see clearly the formation of a three-vortex structure at time $t=50$, emerging for the growth of the most unstable mode $m=3$. However, the phase space structure is unstable and the coalescence of two vortices takes place at time $t=75$. We see indeed that the phase space structures in Fig. 6 that characterize the plasma response caused by both magnetic and electrostatic trapping processes seems to reach a stationary state formed by a two-vortex structure.

As already discussed, the model provides the opportunity of an accurate picture of the instability with respect to the full kinetic approach by looking at the dynamics of each single stream. We focus now on the behaviour of the central stream. Fig. 7 displays the evolution of the central stream at the same times. Even though the main saturation process is the magnetic trapping, at least at the beginning of saturation, the analysis of the behaviour of the particle population of the central beam has revealed novel and surprising features of

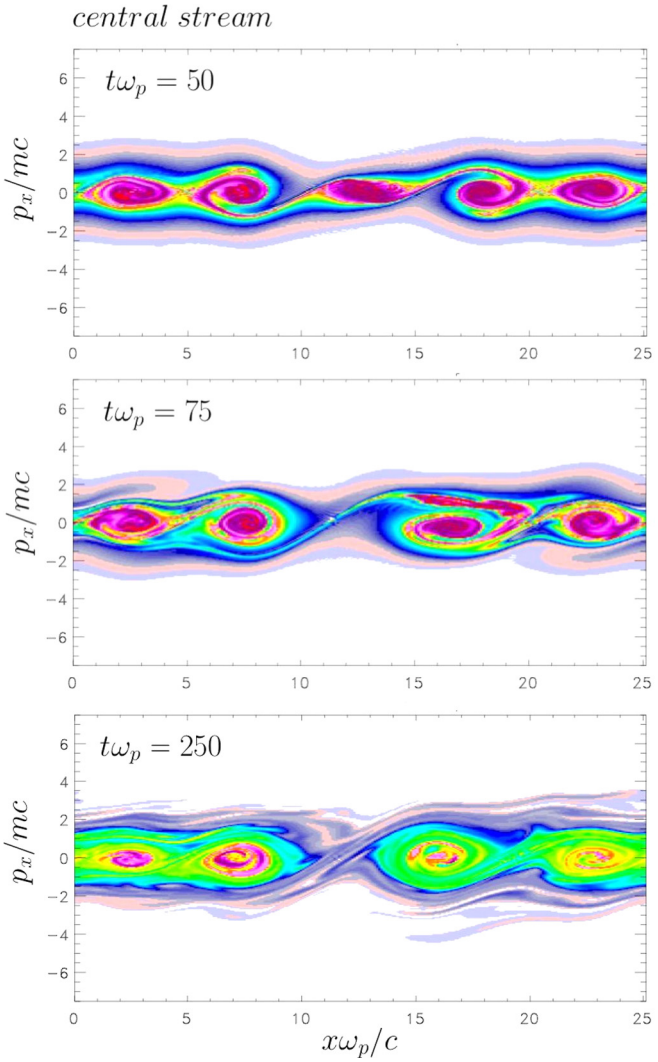

FIG. 7. Phase space representation of the central stream. Particles of the central stream experiences a trapping mechanism induced by the electric potential. The simulation has been performed for $T_\perp \simeq 840$ keV and $\psi = 4$.

the instability. Particles experience also a trapping of electrostatic nature.

One point is especially significant here. Let me consider, for simplicity, a population of resonant particles which experiences only magnetic trapping induced by a strong magnetic field having a dominant mode k_0. Such particles are steadily accelerated and their coherent velocity depends on the elapsed time since phase mixing occurred. Now, the longitudinal electric field in plasma is driven by charge effects (the plasma exhibiting inhomogeneous vortex structures) and grows and it is this self-consistent field that can accelerate individual particles and maintain the stability of the BGK structure provided that the dominant mode for the electric field remains k_0. For the Lorentz force, the dominant mode is $2k_0$. It is the case shown in Figs. 3 and 4 where no vortex merging is observed and the magnetic BGK structure is stable. However, when the growth of the magnetic and electric fields leads of a couple of wave vectors which does not match together with k_0 then the system adjusts itself to satisfy the stability condition of the BGK equilibrium. As a consequence, there is a change in the nature of the initially electron plasma wave, which is no longer a simple Langmuir wave at later times, but, as we hypothesize, a more complex structure characterized by electric trapping effects in the form of phase space "bumps" rather than standard holes met in the non relativistic regime. For instance, the dominant mode, in Figs. 6 and 7, is initially before $t\omega_p \leq 50$, the mode $m = 3$ for the magnetic field and the mode $m = 5$ for the contribution of the Lorentz term in the presence of the electric perturbation. It must be pointed out that it is not the mode $m = 6$ here. Later, the resulting phase space vortex structures turn out to be unstable and not obviously self-sustained and are apparently able to merge together in a pair wise vortex merging process.

By comparing behaviours of the first selected streams on the ring, shown in Fig. 6 with the one of the central stream, it appears that the plasma evolution is now driven by the self-reorganisation of the magnetic field and the electric potential modes in terms of a nonlinear shift to the mode $m = 2$ (or equivalently the mode k_0) and $m = 4$ (i.e., the mode $2k_0$). Our investigation reveals that it is the resonant behaviour of the electrostatic trapping process which determines the resonance condition by imposing the nonlinear shift and the resulting pair wise vortex merging. The choice of the wave number is hardly constrained at all. The resonance is made here on the mode $2k_0$, due to the Lorentz force and where k_0 denotes the dominant mode in the growth of the magnetic field. Thus, if the resonance mode is made on a different mode, the reorganisation of the plasma becomes now possible to reach the equilibrium state, solution of the Vlasov-Maxwell system. On top panel, the behaviour of the central stream is shown at the beginning of the saturation process and it is clear that the selected mode is $m = 5$, different to the expected modes $m = 4$ and $m = 6$ (middle panel in Fig. 7). The mode $m = 5$ is however unstable and a pair wise vortex merging takes place. We found that strong trapping effects occur for even small amplitude electrostatic waves, resulting in undamped stationary waves. The fusion is achieved at time $t\omega_p = 250$. Such a vortex merging has been recently observed in PIC simulations in Ref. 30.

VI. CONCLUDING REMARKS

The multistream model is a very interesting concept which allows us to express, in a simple manner, the property of invariance of the generalized canonical momentum in a perpendicular direction. Starting from the existence of mathematical analogies, we have been able to construct a class of solutions of the reduced Vlasov-Maxwell system in the form of stationary BGK waves in the presence of both electric and magnetic trapping processes. What emerges from the analysis and numerical investigations is the direct result on the particle distribution, of interactions between streams, stemming from the invariance of the canonical momentum. An interesting consequence is the recovery of the quasilinear mechanism where the magnetic bounce frequency for the plasma can be expressed as an average over the particle populations of streams which experience, for each considered stream, their own (local) magnetic trapping scenario. Again, the numerical results confirm that saturation occurs when

this mean magnetic bounce frequency becomes roughly as large as the expected linear mode growth rate, even with a small number of streams.

While the general formalism was reported in Paper I with particular emphasis on the linear behaviour, a detailed analysis of the saturation mechanism is presented here. Within the framework of the multistream theory, a periodic solution, describing the BGK-type solutions, where resonant particles are magnetically and electrically trapped can be only recovered when we consider several streams, so that the calculation may be applied directly to the study of the saturation of the temperature anisotropy driven Weibel instability.

Because the model is fundamentally nonlinear, it turns out to be of more general importance and offers a new approach in the determination of stationary Vlasov-Maxwell solutions in the relativistic regime. In the problem of BGK waves, in their magnetic trapping version, we have shown that even a weak electrostatic contribution can have profound implications for the stability of magnetic vortices and changes the nature of waves. Much more work remains to be done beyond the possibilities afforded by the multistream model, but we hope that the first attempts to characterize the nature of solutions of the set of Vlasov-Maxwell equations can provide guidance and new insight.

On the other hand, from a computational point of view, the multistream model provides a saving factor of order of $N_{p_\perp}/N \sim 10^4$ in the considered case of a circularly polarized wave. First numerical simulations have explored initial conditions constituted by a circular "ring" in perpendicular momentum space with a temporal evolution where the different regimes coexist (purely Weibel instability, coupled electrostatic-magnetic particle trapping, inverse cascade-like instability) illustrating the complexity and the richness of Weibel-type instabilities, that are only grasping owing to the multistream approach.

ACKNOWLEDGMENTS

The author is indebted to the IDRIS computational center, Orsay, France, for computer time allocation on their computers.

APPENDIX: MAGNETIC TRAPPING FEATURES IN STREAM DECOMPOSITION PICTURE

Here, we summarize explicit expressions for the magnetic bounce frequency for a given particle "bunch" in the multistream representation. We assume that there is no electrostatic potential ϕ. Here, dimensionless variables have been defined as $\frac{eA_\perp}{mc} \to \boldsymbol{a}_\perp$, $\frac{eA_0}{mc} \to a_0$, $t\omega_p \to t$, $\frac{x\omega_p}{c} \to x$, $\frac{C_j}{mc} \to \boldsymbol{C}_j$, $\frac{p_x}{mc} \to p_x$. Notice that, in mc^2 units, γ_j denotes also the total energy. We assume a potential vector field in the form (8). Consider the Lorentz factor γ_j be constant and be determined by γ_{0j} (for $p_x = 0$) with $\gamma_{0j} = \sqrt{1 + a_0^2 + C_{\perp j}^2}$. To evaluate the magnetic bounce frequency experienced by a particle population of a given stream j, we start with the equation of motion in the longitudinal direction x

$$\frac{dx}{dt} = \frac{p_x}{m\gamma_j} = \pm\sqrt{\varepsilon_j + \frac{2C_{\perp j}a_0\cos(k_0x - \theta_j)}{\gamma_{0j}^2}} \tag{A1}$$

and where

$$\varepsilon_j = 1 - \frac{1}{\gamma_{0j}^2} - \frac{(C_{\perp j}^2 + a_0^2)}{\gamma_{0j}^2}. \tag{A2}$$

Defining $\rho = k_0x - \theta_j$ where θ_j is a random phase and where we have omitted the index j for simplifying the notation, one obtains then

$$\frac{d\rho}{dt} = k_0\frac{dx}{dt} \tag{A3}$$

and substitute (A3) into (A1) to find, as a function of the ρ variable

$$\frac{1}{k_0^2}\left(\frac{d\rho}{dt}\right)^2 = \frac{2C_{\perp j}a_0(\cos\rho - \cos\rho_0)}{\gamma_{0j}^2}, \tag{A4}$$

where we have introduced ρ_0 defined by

$$\varepsilon_j = \frac{-2C_{\perp j}a_0\cos\rho_0}{\gamma_{0j}^2}. \tag{A5}$$

Moreover, Eq. (A4) can be rewritten in the following form:

$$\frac{\gamma_{0j}^2}{4a_0C_{\perp j}k_0^2}\left(\frac{d\rho}{dt}\right)^2 = \sin^2\frac{\rho_0}{2} - \sin^2\frac{\rho}{2}. \tag{A6}$$

Equation (A6) can be solved in terms of Jacobian elliptic functions by making use of the transformation $\sin\frac{\rho}{2} = \sin\frac{\rho_0}{2}\sin\xi$ and a little algebra leads to

$$\left(\frac{d\psi}{dt}\right)^2 = \frac{C_{\perp j}a_0k_0^2}{\gamma_{0j}^2}\left(1 - \sin^2\frac{\rho_0}{2}\sin^2\xi\right). \tag{A7}$$

By using the usual pitch angle variable $\kappa = \sin\frac{\rho_0}{2}$ where $0 \le \kappa \le 1$, Eq. (A7) becomes

$$\frac{d\xi}{dt} = \pm\sqrt{1 - \kappa^2\sin^2\xi}\sqrt{\frac{C_{\perp j}a_0k_0^2}{\gamma_{0j}^2}} \tag{A8}$$

and the bounce temporal period, for the stream j, driven by magnetic trapping is defined by

$$\tau_{bj} = \frac{2\pi}{\omega_{bj}} = 4\sqrt{\frac{C_{\perp j}a_0k_0^2}{\gamma_{0j}^2}}\int_0^{\frac{\pi}{2}}\frac{d\xi}{\sqrt{1 - \kappa^2\sin^2\xi}} \tag{A9}$$

or equivalently, we have

$$\omega_{bj} = \frac{\pi}{2K(\kappa)}\sqrt{\frac{C_{\perp j}a_0k_0^2}{\gamma_{0j}^2}}. \tag{A10}$$

Here, $K(\kappa) = \int_0^{\frac{\pi}{2}}\frac{d\xi}{\sqrt{1-\kappa^2\sin^2\xi}}$ is the complete elliptic function of first kind. For deeply trapped particles, we can take

$K(0) = \frac{\pi}{2}$ and we recover for ω_{bj} the standard expression given by Eq. (20). The fact that each stream j experiences a different bounce magnetic frequency ω_{bj} appears completely natural when we introduce the conservation of the perpendicular canonical momentum $\boldsymbol{P}_{c\perp} = \boldsymbol{C}_j = const.$

[1]I. Bernstein, J. Greene, and M. D. Kruskal, Phys. Rev **108**, 546 (1957).
[2]W. Bertsch, J. Fajans, and F. Friedland, Phys. Rev. Lett. **91**, 265003 (2003).
[3]A. Ghizzo, B. Izrar, P. Bertrand, E. Fijalkow, M. R. Feix, and M. Shoucri, Phys. Fluids **31**, 72 (1988); E. Siminos, D. Bénisti, and L. Gremillet, Phys. Rev. E **83**, 056402 (2011).
[4]T. W. Johnston, Y. Tyshetskiy, A. Ghizzo, and P. Bertrand, Phys. Plasmas **16**, 042105 (2009).
[5]A. Karmakar, N. Kumar, A. Pukhov, O. Polomarov, and G. Shvets Phys. Plasmas **15**, 120702 (2008).
[6]D. V. Romanov, V. Yu. Bychenkov, W. Rozmus, C. E. Capjack, and R. Fedosejevs, Phys. Rev. Lett. **93**, 215004 (2004).
[7]A. Bret, L. Gremillet, and D. Bénisti, Phys. Rev. E **81**, 036402 (2010).
[8]L. O. Silva, R. A. Fonseca, J. W. Tonge, W. B. Mori, and J. M. Dawson, Phys. Plasmas **9**, 2458 (2002).
[9]M. Lazar, R. Schlickeiser, and P. K. Shukla, Phys. Plasmas **13**, 102107 (2006).
[10]C. Ren, E. G. Blackman, and W. F. Fong, Phys. Plasmas **14**, 012901 (2007).
[11]M. V. Medvedev and A. Loeb, Astrophys. J. **526**, 697 (1999).
[12]M. E. Dieckmann, P. Ljung, A. Ynnerman, and K. G. McClements, Phys. Plasmas **7**, 5171 (2000).
[13]M. E. Dieckmann, Nonlinear Processes Geophys. **15**, 831 (2008).
[14]A. I. Akhiezer and R. V. Polovin, Zh. Eksp. Teor. Fiz. **30**, 915 (1956) [Sov. Phys. JETP **3**, 696 (1956)].
[15]R. L. Berger and R. C. Davidson, Phys. Fluids **15**, 2327 (1972).
[16]M. Lontano, S. V. Bulanov, J. Koga, M. Passoni, and T. Tajima, Phys. Plasmas **9**, 2562 (2002).
[17]M. Lontano, M. Passoni, and S. V. Bulanov, Phys. Plasmas **10**, 639 (2003).
[18]B. Eliasson and P. K. Shukla, Phys. Plasmas **14**, 056703 (2007).
[19]A. Inglebert, A. Ghizzo, T. Reveille, D. Del Sarto, P. Bertrand, and F. Califano, Plasma Phys. Controlled Fusion **54**, 085004 (2012).
[20]A. Inglebert, A. Ghizzo, T. Reveille, P. Bertrand, and F. Califano, Phys. Plasmas **19**, 122109 (2012).
[21]A. Ghizzo and P. Bertrand, Phys. Plasmas **20**, 082109 (2013).
[22]A. Ghizzo, Phys. Plasmas **20**, 082111 (2013).
[23]F. Haas, G. Manfredi, and M. R. Feix, Phys. Rev. E **62**, 2763 (2000).
[24]E. Sonnendrucker, J. Roche, P. Bertrand, and A. Ghizzo, J. Comput. Phys. **149**, 201 (1999).
[25]A. Ghizzo, F. Huot, and P. Bertrand, J. Comput. Phys. **186**, 47 (2003).
[26]S. Zaheer and G. Murtaza, Phys. Plasmas **14**, 072106 (2007).
[27]P. H. Yoon, Phys. Fluids B **1**, 1336 (1989).
[28]P. H. Yoon, Phys. Plasmas **14**, 024504 (2007); H. H. Kaang, C. Mo Ryu, and P. H. Yoon, *ibid.* **16**, 082103 (2009).
[29]R. Schlickeiser, Phys. Plasmas **11**, 5532 (2004); U. Schaefer-Rolffs, I. Lerche, and R. Schlickeiser, *ibid.* **13**, 012107 (2006).
[30]M. E. Innocenti, M. Lazar, S. Markidis, G. Lapenta, and S. Poedts, Phys. Plasmas **18**, 052104 (2011).